electronic reprint

Journal of
Applied Crystallography
ISSN 0021-8898

Peak profile function for synchrotron X-ray diffractometry

T. Ida, H. Hibino and H. Toraya

Journal of
Applied Crystallography
ISSN 0021-8898

Received 18 September 2000
Accepted 22 December 2000

Peak profile function for synchrotron X-ray diffractometry

T. Ida,* H. Hibino and H. Toraya

Ceramics Research Laboratory, Nagoya Institute of Technology, Asahigaoka, Tajimi, Gifu 507-0071, Japan. Correspondence e-mail: ida@crl.nitech.ac.jp

A formula of the instrumental function for a high-resolution synchrotron X-ray diffractometer, equipped with a flat crystal analyser and a set of Soller slits for limiting the axial divergence of the diffracted beam, has been derived. The formula incorporates the effects of (i) the axial divergence of the diffracted beam limited by the Soller slits, (ii) the Bragg angle of the flat crystal analyser, and (iii) the tilt angle defined as the deviation of the normal direction of the analyser face from the goniometer plane. The model profile function given by the convolution of a Lorentzian function with the instrumental function has been applied to fit the experimental diffraction peak profiles of standard Si powder (NIST SRM640b) measured with a high-resolution synchrotron X-ray diffractometer, MDS, on beamline BL4B2 at the Photon Factory in Tsukuba. The convolution has been calculated by applying an efficient algorithm for numerical integration. The profile function reproduces not only the experimental profiles measured with a well aligned crystal analyser, but also significantly distorted profiles arising from misalignment of the analyser, with R_p values within 1.4%, by varying only the instrumental parameter for the tilt angle. It is suggested that further convolution with a Gaussian distribution is practically not necessary for the model instrumental function to fit the data collected with MDS. More rapid computation can be achieved by applying an analytical formula of the profile function, when the tilt angle of the crystal analyser is within about 0.2°.

1. Introduction

By applying synchrotron X-ray radiation with negligible beam divergence to powder diffractometry, most effects of optical aberrations can be removed, while diffractometry with conventional X-ray sources is usually affected by the effects of a flat specimen, sample transparency and displacement of the sample face from the goniometer axis. The effect of axial divergence of the diffracted beam should not be neglected, even in synchrotron X-ray diffractometry, although it is relatively easy to handle in this case compared with the conventional case, in which the axial divergence of both the incident and the diffracted beam should be taken into account simultaneously (Ida, 1998).

Howard (1982) has shown that a model function for asymmetric neutron powder diffraction peaks is given by a convolution of a symmetric function with an asymmetric instrumental function. Laar & Yelon (1984) have proposed a model instrumental function for axial divergence in neutron diffractometry, incorporating the finite lengths of the sample and detector slits along the axial direction. Finger *et al.* (1994) have suggested that the model proposed by Laar & Yelon might be applicable to the profiles measured with a synchrotron X-ray diffractometer, but it seems that there remains ambiguity in the interpretation of the parameters of the model function.

Hastings *et al.* (1984) have proposed a model profile function for a modern high-resolution synchrotron X-ray diffractometer equipped with a crystal analyser on the diffracted-beam side, based on the assumption that the angular distribution of the diffracted beam along the axial direction is expressed by a Gaussian function truncated within the half-maximum region. The basic idea of the model seems to be more appropriate than the treatment by Finger *et al.* (1994). However, treatment of the axial divergence as the truncated Gaussian function is questionable and the optimum value of the axial divergence parameter to fit the experimental profile does not coincide with the angle defined as the ratio of the spacing to the length of the foils of the Soller slits.

We have noticed that the experimental diffraction peak profiles measured with the high-resolution synchrotron X-ray diffractometer MDS (Toraya *et al.*, 1996) on the beamline BL4B2 at the Photon Factory in Tsukuba are considerably deformed when the normal direction of the flat crystal analyser is slightly (1°, for example) tilted out of the goniometer plane. Thus, a mathematical model explicitly including the effect of the tilt angle of the analyser crystal is highly desirable for high-precision analysis of experimental profiles.

In this paper, we derive a geometrically correct formula of the instrumental function for a synchrotron X-ray diffractometer equipped with a flat crystal analyser and a set of Soller slits for limiting axial divergence of the diffracted beam, allowing a slight tilt angle of the analyser. The experimental diffraction peak profiles of standard Si powder (NIST SRM640b) measured with MDS are analysed by a profile fitting method with the model profile function given by the convolution of a Lorentzian function with the instrumental function.

2. Geometric model

2.1. Geometry of diffractometric optics

The geometry of the powder diffractometer is shown schematically in Fig. 1. The horizontal (axial) divergence of the beam diffracted from the specimen is restricted by a set of Soller slits and the detector (scintillation counter) receives the beam that satisfies the Bragg condition at the flat analyser crystal. As shown in Fig. 1, the angles of the goniometer and the analyser are respectively denoted as 2Θ and Θ_A. The diffractometric measurement is conducted by varying 2Θ, while Θ_A is fixed after adjustment to the appropriate angle by a rocking curve measurement for the analyser crystal. Hereinafter, the optical geometry is treated analytically in a coordinate system taking the right direction as the x axis, the upward direction as the y and the forward direction as the z axis, as shown in Fig. 1.

2.2. Tilt angle of the analyser

The diffraction peak profile is affected by the tilt angle Φ_A defined by the angular deviation of the normal direction of the analyser face from the goniometer (xy) plane, while the deviation in Θ_A is expected to cause only constant shift of the peak without deformation of the peak profile.

The normal vector of the analyser, **a**, is expressed by

$$\begin{aligned}\mathbf{a} &= \begin{pmatrix} \cos(2\Theta-\Theta_A) & -\sin(2\Theta-\Theta_A) & 0 \\ \sin(2\Theta-\Theta_A) & \cos(2\Theta-\Theta_A) & 0 \\ 0 & 0 & 1 \end{pmatrix} \\ &\times \begin{pmatrix} 1 & 0 & 0 \\ 0 & \cos\Phi_A & -\sin\Phi_A \\ 0 & \sin\Phi_A & \cos\Phi_A \end{pmatrix} \begin{pmatrix} 0 \\ -1 \\ 0 \end{pmatrix} \\ &= \begin{pmatrix} \sin(2\Theta-\Theta_A)\cos\Phi_A \\ -\cos(2\Theta-\Theta_A)\cos\Phi_A \\ -\sin\Phi_A \end{pmatrix}, \end{aligned} \tag{1}$$

which represents the rotation from the downward direction (0, −1, 0) about the x axis by the angle Φ_A, followed by rotation about the z axis by the angle $2\Theta - \Theta_A$.

2.3. Axial divergence and diffraction condition for a powder sample

Even if the axial divergence of the diffracted beam is restricted by a set of Soller slits, the effect of finite divergence cannot be neglected. When the beam diffracted from the specimen has a Bragg angle of θ, the direction of the beam **b** is expressed by

$$\begin{aligned}\mathbf{b} &= \begin{pmatrix} 1 & 0 & 0 \\ 0 & \cos\varphi & -\sin\varphi \\ 0 & \sin\varphi & \cos\varphi \end{pmatrix} \begin{pmatrix} \cos 2\theta \\ \sin 2\theta \\ 0 \end{pmatrix} \\ &= \begin{pmatrix} \cos 2\theta \\ \sin 2\theta\cos\varphi \\ \sin 2\theta\sin\varphi \end{pmatrix}, \end{aligned} \tag{2}$$

where φ is an arbitrary parameter, when the axial divergence is not restricted.

The angle of axial divergence β is simply related to φ by

$$\tan\beta = \sin 2\theta \tan\varphi. \tag{3}$$

Note that we distinguish the diffraction angle 2θ from the goniometer angle 2Θ by different symbols.

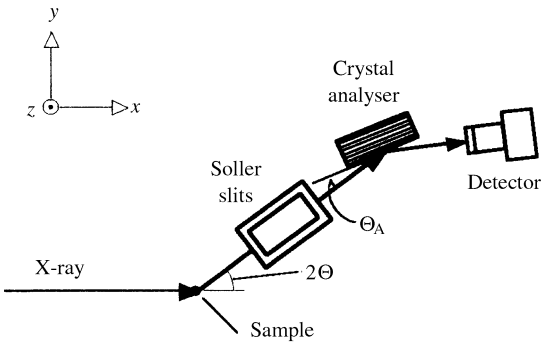

Figure 1
Schematic illustration of the optical geometry of high-resolution synchrotron X-ray diffractometry. 2Θ is the mechanical goniometer angle and Θ_A is the analyser angle. The coordinate system chosen is shown in the upper left part.

2.4. Diffraction condition at the crystal analyser

The diffraction condition at the analyser crystal is that the beam diffracted from the specimen should have an incident angle of Θ_A with respect to the face of the analyser. We assume that the area of the scintillator is wide enough to detect all beams diffracted from the analyser. Then the Bragg condition at the analyser determines the relation between the diffracted beam vector **b** and the normal vector of the analyser, **a**, as follows:

$$\mathbf{b}\cdot\mathbf{a} = \cos(\pi/2 + \Theta_A) = -\sin\Theta_A. \tag{4}$$

2.5. Relation between the axial deviation and the apparent diffraction angles

Here we derive the relation between the diffraction angle 2θ and the goniometer angle 2Θ for the beam axially deviated by the angle β from the goniometer plane.

The definition of the tilt angle, equation (1), the diffraction condition of the powder sample, equation (2), and the

diffraction condition of the analyser crystal, equation (4), immediately give the following exact relation:

$$\begin{aligned}&\sin(2\Theta-\Theta_A)\cos\Phi_A\cos2\theta\\&-\cos(2\Theta-\Theta_A)\cos\Phi_A\sin2\theta\cos\varphi\\&-\sin\Phi_A\sin2\theta\sin\varphi\\&\quad=-\sin\Theta_A.\end{aligned}\tag{5}$$

We define the deviation of the apparent diffraction angle 2θ from the true diffraction angle 2Θ as $\Delta\equiv2\Theta-2\theta$, and derive the second-order Taylor expansion of Δ by φ and Φ_A:

$$\begin{aligned}\Delta\simeq\Delta_0&+\left(\frac{\partial\Delta}{\partial\varphi}\right)_0\varphi+\left(\frac{\partial\Delta}{\partial\Phi_A}\right)_0\Phi_A+\frac{1}{2}\left(\frac{\partial^2\Delta}{\partial\varphi^2}\right)_0\varphi^2\\&+\left(\frac{\partial^2\Delta}{\partial\varphi\partial\Phi_A}\right)_0\varphi\Phi_A+\frac{1}{2}\left(\frac{\partial^2\Delta}{\partial\Phi_A^2}\right)_0\Phi_A^2,\end{aligned}\tag{6}$$

where the subscript 0 indicates the value for $\varphi=0$ and $\Phi_A=0$. It is not difficult to derive the following relations from equation (5):

$$\Delta_0=\left(\frac{\partial\Delta}{\partial\varphi}\right)_0=\left(\frac{\partial\Delta}{\partial\Phi_A}\right)_0=0,\tag{7}$$

$$\left(\frac{\partial^2\Delta}{\partial\varphi^2}\right)_0=-\frac{\cos(2\theta-2\Theta_A)\sin2\theta}{\cos\Theta_A},\tag{8}$$

$$\left(\frac{\partial^2\Delta}{\partial\varphi\partial\Phi_A}\right)_0=\frac{\sin2\theta}{\cos\Theta_A},\tag{9}$$

$$\left(\frac{\partial^2\Delta}{\partial\Phi_A^2}\right)_0=\tan\Theta_A.\tag{10}$$

Therefore, Δ is naturally approximated by

$$\Delta\simeq-\frac{\varphi^2\cos(2\theta-2\Theta_A)\sin2\theta}{2\cos\Theta_A}+\frac{\varphi\Phi_A\sin2\theta}{\cos\Theta_A}+\frac{\Phi_A^2\tan\Theta_A}{2}.\tag{11}$$

Since $\varphi\simeq\beta/\sin2\theta$, as derived from equation (3), Δ is related to the axial deviation angle β by

$$\Delta\simeq-\frac{\beta^2}{2}(\cot2\theta+\tan\Theta_A)+\frac{\beta\Phi_A}{\cos\Theta_A}-\frac{\Phi_A^2}{2}\tan\Theta_A.\tag{12}$$

The first term of the above equation is identical to the formula reported by Hastings *et al.* (1984).

3. Instrumental function for axial divergence

3.1. Transmission function of the Soller slits

The transmission function of the Soller slits is given by the following triangular form:

$$f_{\rm Soller}(\beta)=\begin{cases}(1/\Phi_H)(1-|\beta|/\Phi_H) & \text{for } -\Phi_H<\beta<\Phi_H,\\ 0 & \text{elsewhere},\end{cases}\tag{13}$$

where Φ_H is the axial divergence angle defined as the ratio of the spacing to the length of the foils of the Soller slits.

The instrumental function for the axial divergence is expressed by the following compact formulae:

$$\begin{aligned}w_H(x)&=\int_{-\infty}^{\infty}\delta(x-\Delta)f_{\rm Soller}(\beta)\,{\rm d}\beta\\&=\int_{-1}^{1}\delta(x-Au^2-B'u-C')(1-|u|)\,{\rm d}u\\&=\int_{-1}^{1}\delta[x-A(u+B)^2-C](1-|u|)\,{\rm d}u,\end{aligned}\tag{14}$$

where

$$B\equiv B'/2A,\tag{15}$$

$$C\equiv C'-B'^2/4A,\tag{16}$$

$$A\equiv-(\Phi_H^2/2)(\cot2\theta+\tan\Theta_A),\tag{17}$$

$$B'\equiv\Phi_H\Phi_A\sec\Theta_A,\tag{18}$$

$$C'\equiv-(\Phi_A^2/2)\tan\Theta_A,\tag{19}$$

and $\delta(x)$ is the Dirac delta function. As discussed later, the statistical properties of the instrumental function are directly derived from the above compact formulae.

3.2. Concrete formulae of the instrumental function

In this section, the concrete formulae of $w_H(x)$, as the solution of equation (14), are shown for the case $A\geq0$ and $B\geq0$. The solution for $A<0$ or $B<0$ is given by

$$w_H(x;A,B,C)=w_H(-x;-A,B,-C)\tag{20}$$

and

$$w_H(x;A,B,C)=w_H(x;A,-B,C).\tag{21}$$

In the case $A=0\Leftrightarrow2\Theta=\Theta_A+\pi/2$, the instrumental function $w_H(x)$ is given by

$$w_H(x)=\begin{cases}(1/|B'|)[1-|(x-C')/B'|]\\ \quad\text{for}\quad C'-|B'|<x<C'+|B'|,\\ 0\quad\text{elsewhere}.\end{cases}\tag{22}$$

When $0<A$, the concrete formulae of $w_H(x)$ are:

$$w_H(x)=\begin{cases}[(1-B)/A][(x-C)/A]^{-1/2}\\ \quad\text{for}\quad C<x\leq C+AB^2,\\ (1/A)\{[(x-C)/A]^{-1/2}-1\}\\ \quad\text{for}\quad C+AB^2<x\leq C+A(1-B)^2,\\ (1/2A)\{(1+B)[(x-C)/A]^{-1/2}-1\}\\ \quad\text{for}\quad C+A(1-B)^2<x\leq C+A(1+B)^2,\\ 0\quad\text{elsewhere},\end{cases}\tag{23}$$

for $0\leq B<1/2$;

$$w_H(x) = \begin{cases} [(1-B)/A][(x-C)/A]^{-1/2} \\ \quad \text{for} \quad C < x \le C + A(1-B)^2, \\ (1/2A)\{(1-B)[(x-C)/A]^{-1/2} + 1\} \\ \quad \text{for} \quad C + A(1-B)^2 < x \le C + AB^2, \\ (1/2A)\{(1+B)[(x-C)/A]^{-1/2} - 1\} \\ \quad \text{for} \quad C + AB^2 < x \le C + A(1+B)^2, \\ 0 \quad \text{elsewhere}, \end{cases} \tag{24}$$

for $1/2 \le B < 1$; and

$$w_H(x) = \begin{cases} (1/2A)\{-(B-1)[(x-C)/A]^{-1/2} + 1\} \\ \quad \text{for} \quad C + A(B-1)^2 < x \le C + AB^2, \\ (1/2A)\{(B+1)[(x-C)/A]^{-1/2} - 1\} \\ \quad \text{for} \quad C + AB^2 < x \le C + A(B+1)^2, \\ 0 \quad \text{elsewhere}, \end{cases} \tag{25}$$

for $1 \le B$.

Figs. 2 and 3 show the variation of the shape of the instrumental function $w_H(x)$ for some realistic values of diffraction angle 2θ, analyser angle Θ_A, axial divergence angle Φ_H and analyser tilt angle Φ_A.

It is found that not only the shift and broadening, but also the asymmetry of the peak is significantly affected by the finite values of the tilt angle Φ_A in the case of low diffraction angle. The peak-top position may shift to the higher angle as a result of the effect of the tilt angle, as shown in the profiles in Fig. 2, while the centroid always shifts to the lower angle, as will be discussed in the following section.

When the diffraction angle is near $(90^\circ + \Theta_A)$, the shift and broadening of the peak become the main effects of finite Φ_A, as shown in Fig. 3.

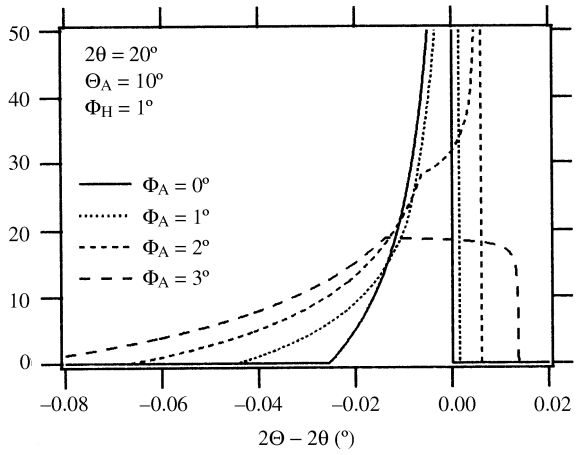

Figure 2
Profiles of the instrumental function $w_H(x)$ for the case $2\theta = 20^\circ$. Θ_A is the analyser angle, Φ_H is the axial divergence angle and Φ_A is the tilt angle of the analyser.

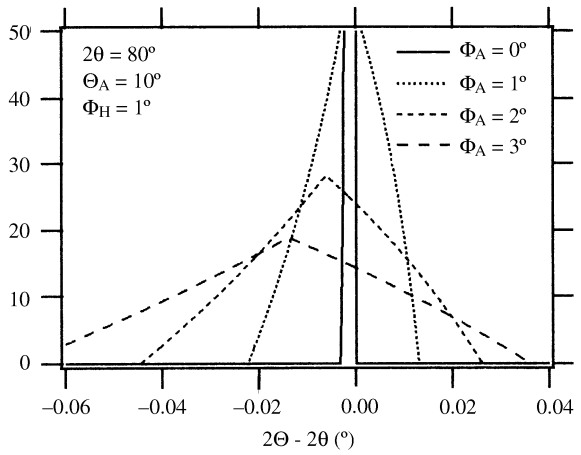

Figure 3
Profiles of the instrumental function $w_H(x)$ for the case $2\theta = 80^\circ$. See Fig. 2 for definitions.

When the crystal analyser is precisely adjusted and the effect of the tilt angle Φ_A is negligible, the instrumental function has the following simple formula:

$$w_H(x) = \begin{cases} (1/|A|)[(x/A)^{-1/2} - 1] & \text{for} \quad 0 < x/A \le 1, \\ 0 & \text{elsewhere.} \end{cases} \tag{26}$$

3.3. Statistical properties of the instrumental function

The mean, x_H, and the variance, σ_H^2, of the instrumental function $w_H(x)$, defined by

$$x_H \equiv \int_{-\infty}^{\infty} x\, w_H(x)\, \mathrm{d}x, \tag{27}$$

and

$$\sigma_H^2 \equiv \int_{-\infty}^{\infty} (x - x_H)^2 w_H(x)\, \mathrm{d}x, \tag{28}$$

respectively, are easily calculated from equation (14) rather than from the results presented in the previous section.

The statistical mean of the instrumental function is derived as follows:

$$\begin{aligned} x_H &= \int_{-\infty}^{\infty} x \int_{-1}^{1} \delta(x - Au^2 - B'u - C')(1 - |u|)\, \mathrm{d}u\, \mathrm{d}x \\ &= \int_{-1}^{1} (1 - |u|) \int_{-\infty}^{\infty} x\delta(x - Au^2 - B'u - C')\, \mathrm{d}x\, \mathrm{d}u \\ &= \int_{-1}^{1} (1 - |u|)(Au^2 + B'u + C')\, \mathrm{d}u \\ &= A/6 + C' \\ &= -(\Phi_H^2/12)(\cot 2\theta + \tan \Theta_A) - (\Phi_A^2/2) \tan \Theta_A. \end{aligned} \tag{29}$$

The above equation shows that the average shift of the peak consists of the terms proportional to the squared axial divergence Φ_H^2 and the squared tilt angle Φ_A^2, the latter of which is

independent of the diffraction angle 2θ and always causes a shift to the lower angle.

The variance is similarly given by

$$\sigma_H^2 = 7A^2/180 + B'^2/6 = (7\Phi_H^4/720)(\cot 2\theta + \tan\Theta_A)^2 + (\Phi_H^2\Phi_A^2/6)\sec^2\Theta_A. \quad (30)$$

The broadening arising from the tilt angle Φ_A, which is given by the second term of the above equation, is also found to be independent of 2θ.

4. Model profile function as a convolution

4.1. Symmetric profile function

We assume that the experimental diffraction peak profiles are modelled by the convolution of a symmetric profile function with the instrumental function. The effect of finite size of crystallites on the diffraction peak broadening is empirically known to have a Lorentzian distribution (Keijser *et al.*, 1982), while the basic resolution function of the optics is expected to be approximated by a Gaussian function (Rietveld, 1969). Thus it seems that the Voigt profile function defined as the convolution of Lorentzian and Gaussian functions is the most natural description of the symmetric feature of the profile function. However, our preliminary investigations on the experimental peak profiles of standard Si powder (NIST SRM 640b) measured with MDS have shown that the observed peak profiles are well reproduced by a convolution of a Lorentzian function,

$$f_L(x) = (1/\pi\gamma_L)[1 + (x/\gamma_L)^2]^{-1}, \quad (31)$$

with the instrumental function $w_H(x)$; the Gaussian distribution is practically negligible. Neglecting the Gaussian distribution, a numerically precise evaluation of the convolution can easily be achieved as described in the following section.

4.2. Calculation of convolution

4.2.1. Convolution of a Lorentzian function with the general formula of instrumental function. The profile function defined as the convolution of a Lorentzian function $f_L(x)$ with the instrumental function $w_H(x)$ is given by

$$p(x) = f_L(x) \otimes w_H(x) = \int_a^b f_L(x-y)w_H(y)\,dy, \quad (32)$$

where a and b are respectively the lower and upper limits of the variable having non-zero values of the instrumental function $w_H(x)$.

As the instrumental function is given as a piecewise analytical function, the integral range is divided into two or three regions according to the cases presented in §3.2. The total convolution is expressed by

$$p(x) = \sum_{i=1}^{M} q_i(x), \qquad q_i(x) = \int_{a_{i-1}}^{a_i} f_L(x-y)w_H(y)\,dy, \quad (33)$$

where $a_0 \equiv a$ and $a_M \equiv b$. The numerical evaluation of each integral $q_i(x)$ is efficiently conducted by applying the following formulae (Ida & Kimura, 1999):

$$q_i(x) \simeq (\alpha_i - \alpha_{i-1})\frac{F_L(x-y_0)}{x-y_0}\sum_{j=1}^{N}\frac{w_j w_H(y_j)}{w_H[W_H^{-1}(\xi_j)]}, \quad (34)$$

where $F_L(x)$ is the primitive function of $f_L(x)$, *i.e.*

$$F_L(x) = (1/\pi)\arctan(x/\gamma_L), \quad (35)$$

$W_H(x)$ is the primitive function of $w_H(x)$,

$$y_j = x - F_L^{-1}\left\{\frac{F_L(x-y_0)}{x-y_0}\left[x - W_H^{-1}(\xi_j)\right]\right\}, \quad (36)$$

$$\alpha_i = W_H\left[x - \frac{x-y_0}{F_L(x-y_0)}F_L(x-a_i)\right], \quad (37)$$

$$\xi_j = \alpha_{i-1} + (\alpha_i - \alpha_{i-1})x_j, \quad (38)$$

x_j and w_j are the abscissa and weights of an N-term Gauss–Legendre integral (Press *et al.*, 1986), and y_0 is chosen as the most significant point for the instrumental function, *i.e.* the point where $w_H(x)$ has the maximum value in each divided integral region. A 16-term ($N = 16$) Gauss–Legendre integral gives almost exact results for any combination of realistic values of the parameters.

4.2.2. Profile function for negligible tilt angle. The convolution of a Lorentzian function with the formula of the instrumental function for negligible tilt angle, equation (26), has an analytical solution expressed by a combination of elementary functions as follows:

$$p(x;\gamma_L,A) = (1/\gamma_L)f_{LH}(x/\gamma_L, A/\gamma_L), \quad (39)$$

$$f_{LH}(u,v) = (1/2\pi wp)\ln[(v+p+w)/(v-p+w)] + (1/\pi wq)\{\pi/2 - \arctan[(w-v)/q]\} - (1/\pi v)\{\pi/2 - \arctan[(1+u^2)/v - u]\} \quad \text{for} \quad v > 0, \quad (40)$$

with

$$f_{LH}(-u,-v) = f_{LH}(u,v), \quad (41)$$

where $w \equiv (u^2+1)^{1/2}$, $p \equiv [2v(w+u)]^{1/2}$, $q \equiv [2v(w-u)]^{1/2}$. As the above formulae include only three square-roots, one logarithm and two arctangents (apart from arithmetic operations), they will be computed more rapidly and safely than the numerical evaluation described in the previous section.

5. Analysis of experimental profiles

5.1. Experimental

The experimental diffraction peak profiles of standard Si powder (NIST SRM 640b) were collected with a high-reso-

lution synchrotron powder X-ray diffractometer, MDS (Toraya *et al.*, 1996), on beamline BL4B2 at the Photon Factory in Tsukuba. The Si powder was loaded into a cylindrical aluminium sample holder, which was mounted on an attachment rotated, at about one revolution s^{-1}, about the normal to the sample surface during measurements. The diffractometer is equipped with a set of Soller slits, with an axial divergence angle $\Phi_H = 1^\circ$, and a Ge(111) crystal analyser (d_{111} = 3.26638 Å) adjusted at $\Theta_A = 6.2^\circ$ for the wavelength 0.707 Å on the diffracted-beam side. The incident X-ray beam was restricted to 2.5 mm in width and 1 mm in height with a couple of slits on the incident-beam side.

The full width at half-maximum (FWHM) value of the rocking curve for the Ge(111) analyser, measured by scanning 2Θ around zero with an attenuated direct beam, was estimated to be about 0.005°, which is close to the value reported by Hastings *et al.* (1984).

5.2. Analysis

The observed 111, 220 and 311 reflection peaks of Si have been fitted simultaneously by a least-squares method with the profile function defined by the convolution of a Lorentzian function with the instrumental function, which is evaluated by a 16-term numerical integral for each divided region. The analyser angle and the axial divergence angle were fixed at $\Theta_A = 6.2^\circ$ and $\Phi_H = 1^\circ$.

The position $2\theta_i$, the integrated intensity I_i and the Lorentzian FWHM value w_i of each peak (i = 1, 2,3), the tilt angle of the analyser Φ_A, and the background parameters b_0, b_1 and b_2, are treated as independent variable parameters in the fitting.

The overall profiles are given by

$$Y(x)_{\rm calc} = \sum_{j=0}^{2} b_j (x - 2\theta_1)^j + \sum_{i=1}^{3} I_i p_i(x) \qquad (42)$$

and

$$p_i(x) = f_L(x - 2\theta_i; w_i/2) \otimes w_H(x; 2\theta_i, \Theta_A, \Phi_H, \Phi_A). \qquad (43)$$

The experimental profiles observed in two different measurement runs have been analysed. The first measurement was conducted with an accidentally tilted analyser, the apparent tilt angle of which was 1.0 (1)°, while the second was measured after the tilt angle of the analyser had been carefully adjusted to 0.0 (1)°.

The results of the profile fittings are shown in Figs. 4 and 5, and listed in the second and third columns of Table 1. The R factors for profile fitting, $R_{\rm wp}$ and R_p, defined by

$$R_{\rm wp} = \left\{ \frac{\sum_i w_i [Y(2\theta_i)_{\rm obs} - Y(2\theta_i)_{\rm calc}]^2}{\sum_i w_i Y(2\theta_i)_{\rm obs}^2} \right\}^{1/2}, \qquad (44)$$

and

$$R_p = \frac{\sum_i |Y(2\theta_i)_{\rm obs} - Y(2\theta_i)_{\rm calc}|}{\sum_i Y(2\theta_i)_{\rm obs}}, \qquad (45)$$

respectively, are also listed in Table 1.

It should be emphasized that the variations of the three experimental peak profiles, strongly dependent on the diffraction angle 2θ, are all well reproduced by the model function, applying the common values of the instrumental parameters Φ_H and Φ_A, which supports the validity of the current model for the instrumental function. The excellently small R values of $R_{\rm wp}$ = 2.0–2.1% and R_p = 1.3–1.4%, and the nearly statistical behaviour of the deviation shown in the difference plot, mean that almost all the information in the experimental profiles has already been extracted by the profile function. It is suggested that further convolution with a Gaussian distribution is practically not necessary for the current model instrumental function to fit the experimental data collected with MDS.

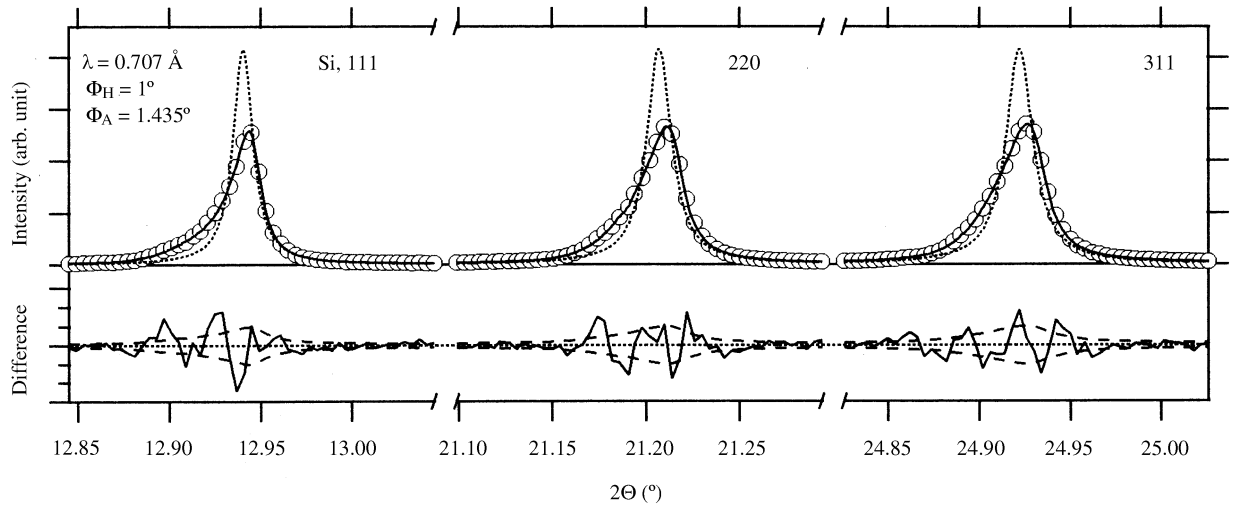

Figure 4
Synchrotron diffraction data for 111, 220 and 311 reflections from Si (NIST SRM 640b) collected with 0.707 Å X-rays and a Ge(111) analyser accidentally tilted by an angle of about 1°. Open circles in the upper part are the experimental points, the solid line is the least-squares fit and the dotted line is the extracted Lorentzian component. The lower part shows the difference plot (solid line) with the standard uncertainties (dashed line) of the data, drawn on a magnified scale.

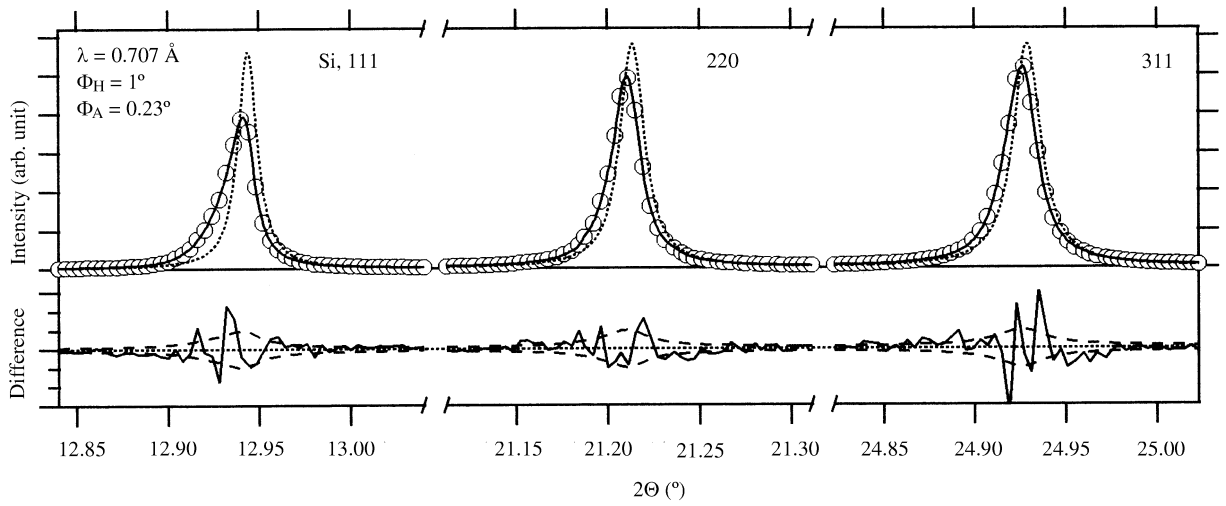

Figure 5
Synchrotron diffraction data for 111, 220 and 311 reflections from Si (NIST SRM 640b) collected with 0.707 Å X-rays and a well aligned Ge(111) analyser. See Fig. 4 for symbolism.

The significant distortion of the experimental profiles, showing broadening and enhanced asymmetry, for the tilted analyser are well simulated by varying only the instrumental parameter Φ_A in the model profile function. The difference in the values of Φ_A, estimated as 1.435 (7) and 0.23 (2)°, coincides with the apparent tilt angle of the analyser, within experimental uncertainty.

From equation (30), the line broadening effect for the values $\Theta_A = 6.2°$, $\Phi_H = 1°$ and $\Phi_A = 0.23°$, is roughly evaluated in terms of Gaussian FWHM value as

$$2[(\ln 2)/3]^{1/2}\Phi_H\Phi_A \sec\Theta_A \simeq 0.004°, \qquad (46)$$

which is close to the FWHM value of the rocking curve, 0.005°. However, it is difficult to express clearly how the width of the rocking curve, which is affected by spectral width and divergence of the source X-ray, as well as mosaicity and strain in the analyser crystal (Hastings *et al.*, 1984), propagates into the powder diffraction peak profile. It may contribute not only to the parameter Φ_A but also to the Lorentzian width w_j in the current model profile function.

The Lorentzian components extracted by the profile fitting are plotted as dotted curves in the upper parts of Figs. 4 and 5. Although the experimental profiles observed in the two measurement runs are quite different, the estimated Lorentzian widths w_j show very good coincidence within the standard uncertainties as listed in Table 1; that is, the shapes of the Lorentzian components extracted by the profile fittings for the two different measurement runs are virtually identical.

If the value of the tilt angle is negligible, the analytical form of the profile function, equation (39), will be applicable. The results of fitting by the analytical profile model to the experimental data collected with a well aligned analyser are listed in the fourth column of Table 1. Though the R factors have been slightly increased, the estimated intensities I_j have coincided with the results obtained by the general profile model within the standard uncertainties. Although systematic differences beyond the standard uncertainties are found in the peak location $2\theta_j$ and the Lorentzian width w_j, the angular difference, about 0.0001°, will usually be negligible.

Since the computation of the analytical formula is faster than the numerical form, it will be more convenient for application to Rietveld analysis or the whole-pattern fitting method.

Table 1
Profile parameters estimated by a least-squares method.

$2\theta_{hkl}$, I_{hkl} and w_{hkl} are respectively the position, the integrated intensity and the Lorentzian FWHM value of each peak. Φ_A is the tilt angle of the analyser. b_j (j = 0, 1, 2) are the background parameters.

	Misaligned analyser	Well aligned analyser	
	Numerical model	Numerical model	Analytical model
$2\theta_{111}$	12.94010 (6)	12.94375 (4)	12.94386 (4)
I_{111}	421 (2)	561 (2)	561 (2)
w_{111}	0.0128 (2)	0.01272(9)	0.01281 (9)
$2\theta_{220}$	21.20680 (6)	21.21339 (4)	21.21351 (3)
I_{220}	807 (3)	795 (3)	797 (3)
w_{220}	0.0157 (2)	0.01565 (9)	0.01587 (8)
$2\theta_{311}$	24.92175 (4)	24.92893 (4)	24.92904 (4)
I_{311}	1618(4)	1657(4)	1661(4)
w_{311}	0.0177 (2)	0.01791 (8)	0.01817 (6)
Φ_A	1.435 (7)	0.23 (2)	0 (fixed)
b_0	22 (4)	21 (4)	20 (4)
b_1	−18 (3)	−14 (3)	−13 (3)
b_2	2.9 (3)	2.8 (3)	2.7 (3)
R_{wp} (%)	2.11	2.04	2.16
R_p (%)	1.34	1.39	1.49

5.3. Accuracy of the numerical calculation

Finally, the accuracy of the numerical evaluation of the convolution is tested by applying a decreased number of terms of the numerical integral. The differences between the experimental data measured with a well aligned analyser and the curves calculated with the same profile parameters as listed in the third column of Table 1, are evaluated in terms of the R factors. The dependence of R_{wp} and R_p values on the number of terms N is represented in Table 2.

Table 2
The dependence of R_{wp} and R_p values on the number of terms N of numerical integration for each divided region.

The profile parameters listed in the third column of Table 1 were used for calculation.

N	R_{wp} (%)	R_p (%)
1	8.41	6.90
2	3.95	2.84
4	2.27	1.50
8	2.07	1.41
16	2.04	1.39

The R values rapidly decrease and approach to convergence on increasing N. It is suggested that $N = 4$ is useful for rough estimation and $N = 8$ will give practically sufficient precision. As the convolution is calculated by two or three divided regions, high-precision evaluation of the total profile function can by achieved only by use of a 16- to 24-term numerical integration.

6. Conclusions

High-resolution synchrotron X-ray powder diffraction peak profiles are satisfactorily reproduced by the convolution of a Lorentzian function with a correct instrumental function incorporating the tilt angle of the analyser crystal.

When the analyser is well aligned and the tilt angle is negligible, a rapid analytical formula of the model profile function is applicable. Even if the profile is significantly distorted as a result of misalignment of the analyser crystal, the general model profile function, precisely calculated by numerical integration employing only 16 to 24 terms, will be useful for Rietveld analysis or the whole-pattern fitting method.

References

Finger, L. W., Cox, D. E. & Jephcoat, A. P. (1994). *J. Appl. Cryst.* **27**, 892–900.
Hastings, J. B., Thomlinson, W. & Cox, D. E. (1984). *J. Appl. Cryst.* **17**, 85–95.
Howard, C. J. (1982) *J. Appl. Cryst.* **15**, 615–620.
Ida, T. (1998). *Rev. Sci. Instrum.* **69**, 2268–2272.
Ida, T. & Kimura, K. (1999). *J. Appl. Cryst.* **32**, 982–991.
Keijser, Th. H. de, Langford, J. I., Mittemeijer, E. J. & Vogels, A. B. P. (1982). *J. Appl. Cryst.* **15**, 308–314.
Laar, B. van & Yelon, W. B. (1984). *J. Appl. Cryst.* **17**, 47–54.
Press, W. H., Flannery, B. P., Teukolsky, S. A. & Vetterling, W. T. (1986). *Numerical Recipes.* Cambridge University Press.
Rietveld, H. M. (1969). *J. Appl. Cryst.* **2**, 167–173.
Toraya, T., Hibino, H. & Ohsumi, K. (1996). *J. Synchrotron Rad.* **3**, 75–83.